Paper bending stiffness and web tension measurement from a running web using a vacuum and computer imaging

MIKKO SALO, ANNA-LEENA ERKKILÄ, MATTI VILKKO, AND MIKKO KANERVA

ABSTRACT: A novel method for measuring the bending stiffness of paper online during manufacturing is introduced. The method uses photometric stereo imaging to detect the shape of the deflection surface caused by a controllable pressure difference over the paper's surfaces. The hardware for the measurement is based on a combination of two existing sensors, which has accelerated and facilitated the development of the implementation. The deflection and loads are tied together by the governing differential equation for the bending of an orthotropic elastic plate with selected simplifications. An approach to resolve material parameters and in-plane loads without knowledge of traditional boundary conditions is suggested.

The presented method was tested in a paper mill during manufacturing. For bending stiffnesses measured online, correlation coefficients 0.88 and 0.92 were obtained compared to state-of-the-art laboratory measurements. However, the results gained from a moving web are noisy and the data requires correction of the slope and an offset. Although several issues remain to be resolved before the method can be considered as an accurate measurement for industrial use, the theoretical background, the performance of online implementation, and the results are promising. Possible causes for the observed discrepancies and the future development of the method are discussed.

Application: In this study, the reader is introduced to a proposed novel method for measuring paper bending stiffness. The study is related to the field of papermaking, as online strength measurements have been studied in the past, but not widely accepted for use by the industry.

The demand for packaging paperboard and cardboard is rising, and packaging applications are the largest use of paper. The industry uses high amounts of energy and other resources; hence, it is subject to environmental debate [1]. Optimized manufacturing processes can reduce the environmental impact of the industry. The mechanical properties of paper are generally only measured after the product has been made. For this reason, raw materials are being excessively used to meet the requirements. Paperboard produced in a paper mill has different mechanical properties in different directions. In the machine direction (MD), tensile properties are higher than those in the cross-machine direction (CD), since most fibers are oriented in MD. The formation of the web and in-plane load (so-called tension) difference in MD and CD during drying are some of the causes of this anisotropy. For paper, the material behavior can be different in tension than in compression due to the nature of the fiber network [2].

Bending stiffness is one of the major quality parameters of paperboard and containerboard, and its functions are to provide physical protection to the contents of a package. Stiffness is also a critical parameter for conversion and a packaging line's efficiency. For the paperboard manufacturer, it is important to achieve consistent (maximum) stiffness with the lowest possible grammage to support cost-effective and sustainable packaging. The current state-of-the-art technology for measuring the various elastic properties of paperboard are standardized off-line laboratory techniques, such as tensile test, short span compression strength (SCT), ring crush test (RCT), and bending stiffness as assessed by, for example: ISO 1924 "Paper and board — Determination of tensile properties — Part 2: Constant rate of elongation method (20 mm/min)," TAPPI T 494 "Tensile properties of paper and paperboard (using constant rate of elongation apparatus)," ISO 9895 "Paper and board — Compressive strength — Short-span test," TAPPI T 826 "Short span compressive strength of containerboard," ISO 12192 "Paper and board — Determination of compressive strength — Ring crush method," TAPPI T 822 "Ring crush of paperboard (rigid support method)," and ISO 5628 "Paper and board — Determination of bending stiffness — General principles for two-point, three-point and four-point methods." An ultrasonic technique for determining stiffness is also commonly used.

There have also been extensive attempts to develop online mechanical testing using contacting methods, such as loading wheel [3-5] and ultrasonic sensors [6-10], as well as non-contacting laser-ultrasonic and interferometer techniques [11, 12]. Various challenges have arisen; for example, challenges with repeatability, high scatter, noise, online

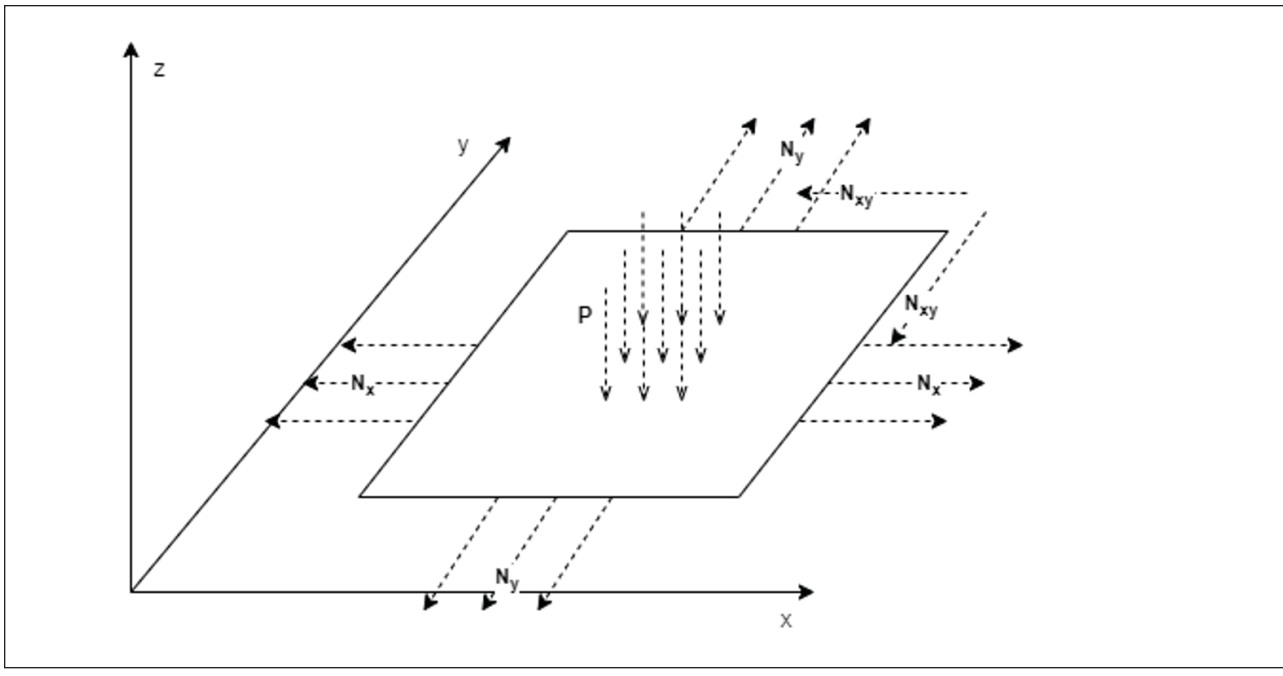

1. Diagram of a plate under transverse load,* p*, and in-plane loads,* N*, acting in the middle plane of the plate.

deployment, frequent need for calibration, and complications with theoretical basis [5,6,8,11]. So far, none of these methods has widely spread for industrial use.

This paper proposes a novel method for measuring the bending stiffness. The method also allows solving for paper's tension in a running web. The solution is based on the theory of plates. The measurement unit consists of two fundamental parts, both of which are based on existing commercial online sensors:

1. The load to locally deflect paper is applied via vacuum by utilizing the Valmet IQ Porosity sensor (Valmet; Espoo, Finland).
2. The shape of the deflected surface is detected using the Valmet IQ Surface sensor.

Both sensors have been slightly modified to meet the requirements of the measurements. Since the sensors are already in commercial use, the online implementation is straightforward. The theory, instruments, and the results from a trial with the first production machine are presented in this paper. Further development of the measuring arrangement and the analysis method is in progress, and some current topics and future plans are discussed.

METHODS

Proposed method

The bending stiffness of a thin plate is solved using known surface shape, known transverse load distribution, and a plate bending model. The discretized height profile, $w(x,y)$, of the plate is obtained using photometric stereo. The details of this method are discussed in Appendix A.

The partial differential equation for plate bending is:

$$q = D_x \frac{\partial^4 w}{\partial x^4} + 2(D_1 + 2D_{xy}) \frac{\partial^4 w}{\partial x^2 \partial y^2} + D_y \frac{\partial^4 w}{\partial y^4} - N_x \frac{\partial^2 w}{\partial x^2} - 2N_{xy} \frac{\partial^2 w}{\partial x \partial y} - N_y \frac{\partial^2 w}{\partial y^2}. \quad (1)$$

The detailed definitions of the material model leading up to Eq. 1 are discussed in Appendix B. The plate's constants, D, are called the bending stiffness (or flexural rigidity) per direction of the plate. N_x, N_y, and N_{xy} are the in-plane loads. The transverse load distribution, $q(x,y)$, can vary for different locations of the considered surface, and it contains the weight of the plate whenever gravity is included. For traditional problems with plates, boundary conditions are required to solve the differential Eq. 1. Alternatively, reverse engineering may be used to solve for the plate's properties (D) and loads (N) when w and q are known based on measurements. **Figure 1** illustrates the plate and the loads affecting it.

Validation method

State-of-the-art measurements by Valmet Paper Lab are used for validation of the proposed method. PaperLab measures the tensile stiffness, T, of the material according to ISO 1924:2005. The single sheet thickness of the material, h, is measured according to ISO 534:2011 "Paper and board — Determination of thickness, density and specific volume." The bending stiffness, D, is then solved from:

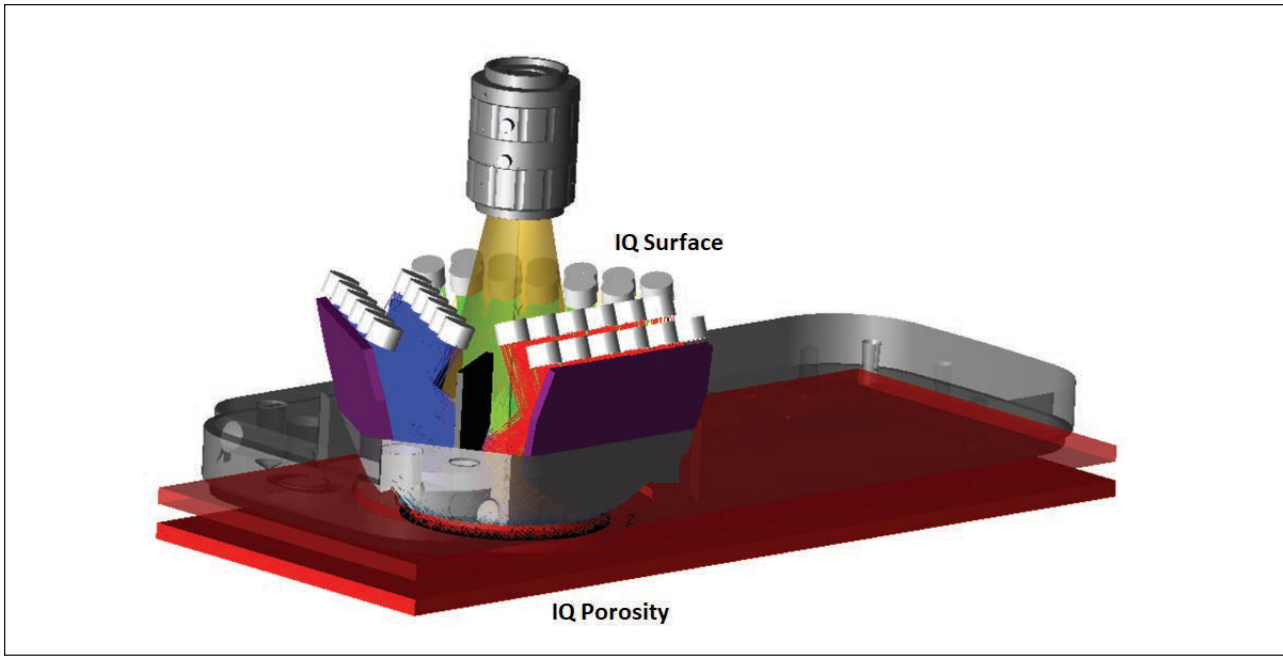

2. Scheme of the novel measurement system prototype. The IQ Surface sensor is visible on the top, and the IQ Porosity sensor resides underneath the bottom of the red plate. The paper web runs between the red plates.

$$D = \frac{Th^2}{12} \quad (2)$$

The measurements are conducted on test strips cut longitudinally from the manufactured product along both CD and MD separately.

EXPERIMENTAL

Hardware and architecture

The methods described previously are used to estimate the bending stiffness, *D*, of paperboard. The paperboard is considered a thin plate. The transverse load distribution, *q*, as in the previous section, is locally created by a measurable pressure difference (vacuum in the event of negative difference). The forces, *N*, acting on the plane in the middle of the plate represent the momentary web tension of the paper machine. It is noteworthy that the tensions solved with our method represent the tension in a very localized region rather than the entire web.

A prototype of the measurement system has been created by Valmet Automation. The system is mounted in the Valmet IQ Quality Control System (QCS) scanner, which scans in the width direction of the paper web at speeds around 0.2–0.5 m/s while making various local measurements. The prototype consists of a porosity meter, a camera, and LED lighting. The prototype is depicted in **Fig. 2**.

The porosity meter is designed to measure the porosity of paper online by generating a measurable and controllable pressure difference over the surface of the paper using suction (leading to vacuum at the sensor point). The measurement vacuum is applied through a circular hole with a diameter of 23 mm in a metal plate. The device also features so-called "hold vacuum" at the edges. This is used to hold the paperboard in contact with the porosity meter and planar in the measurement plane, as shown in **Fig. 3**, when the measurement vacuum is not used. The hold vacuum does not deform the surface in the sensor location. The vacuum pressure experienced by the paper is set low enough, around 3–12 kPa, depending on the weight of the product, to not cause permanent deformations to the product, making the measurement viable for online use.

The IQ Surface-sensor is designed to measure surface roughness by means of photometric stereo, utilizing a camera and a set of red, green, and blue (RGB) lights. In the measurement of the shape of the deflected area, larger scale variations are of interest. The positions of the camera and light sources were adjusted accordingly. The camera provides images of the surface with a resolution of 1392 pixels x 1392 pixels from an area of 34.8 mm² x 34.8 mm² and can capture and process at least 10 images per second. The RGB LED lights are used to illuminate the surface from different, known directions.

The images from the camera are divided into two categories: reference images and sample images. Reference images are taken of a planar surface with zero measurement vacuum and are used to correct the optical system conditions. The hold vacuum may be used during acquisition of reference images so that the paper resides as close to the measurement plane as possible. The sample images are taken when the measurement vacuum pressure is applied and the data is used to calculate the resulting surface shape,

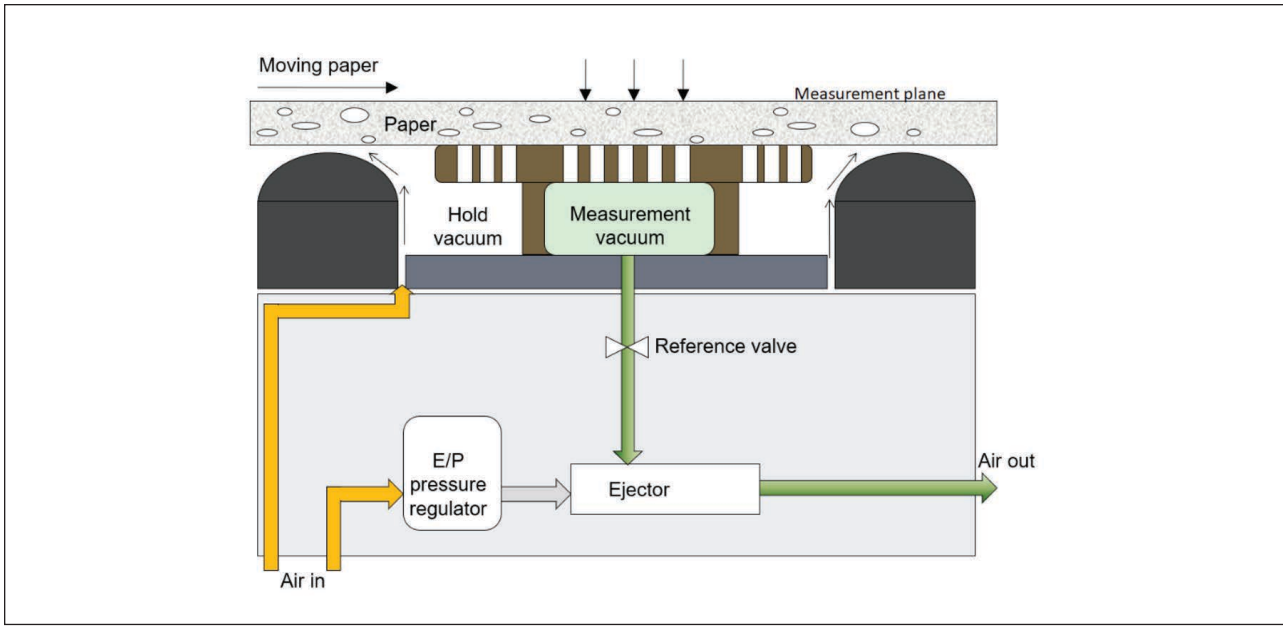

3. Scheme of the porosity meter (picture by Valmet Automation).

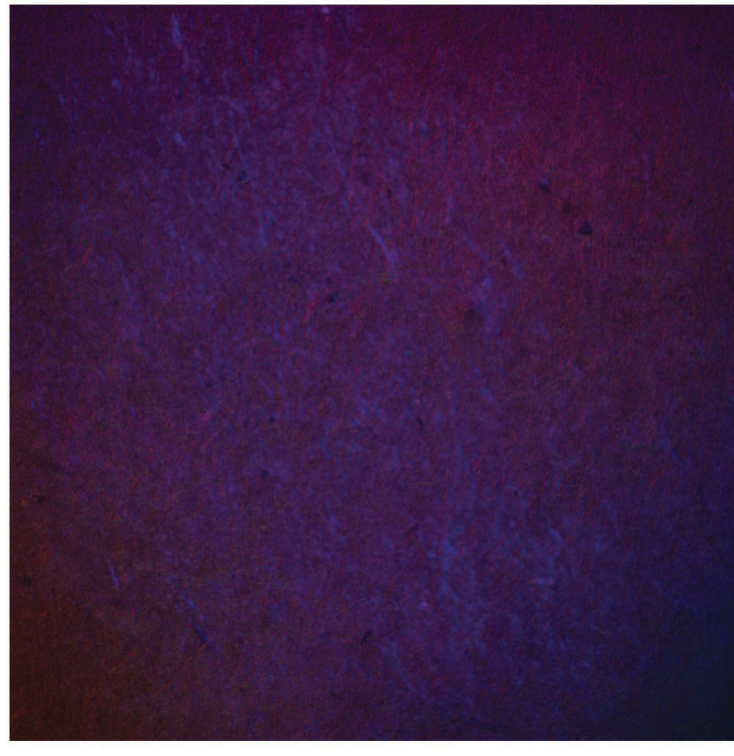

4. An unfiltered raw image from the camera. Fibers (light lines) and moisture (dark spots) are clearly visible, as they refract light in a different way.

after the optical system conditions have been normalized. The surface of paperboard contains cellulose fibers that have significantly different colors, and these appear in different locations in each consecutive image. The situation is depicted in **Fig. 4**. This causes shapes in the calculated surface that are not due to physical surface form, but rather due to different colors of the surface material refracting light at different intensities. Another source of detrimental small-scale surface shape variations is the surface structure and topography of paperboard resulting from roughness, flocs, and thickness variations. The effect of these stochastic variations in albedo and small-scale topography can be

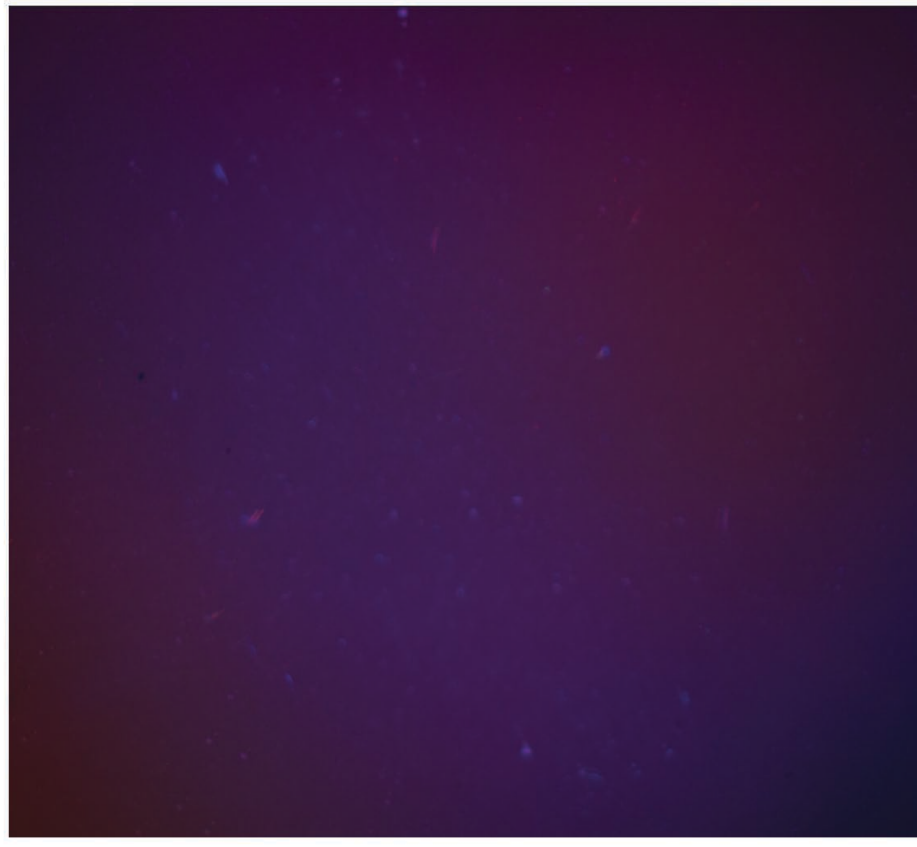

5. Mean of 310 images. The fibers have been averaged out. The remaining spots are static and in the optical system.

reduced by mean-filtering both the reference and sample images between successive images. The resulting mean of each pixel in each color channel is used in calculations. An example of a mean filtered image is shown in **Fig. 5**.

Once the mean-filtering and reference correction is done, the resulting image is again low-pass filtered, for example, using discrete orthogonal polynomial fitting or Fourier transforms to remove any remaining noise and other variations (e.g., there could be a smudge in the lens that occurred between the reference and sample images). The resulting image is used to determine the first partial derivatives of the surface height (w) in the x- and y-directions. The partial derivatives are used either directly to calculate the higher order derivatives or integrated into a surface first using Fourier transform. An integrated surface obtained from the photometric stereo is depicted in **Fig. 6**. The higher order derivatives needed in the system of equations in Eq. 1 are calculated using the three-point centered difference formula. They may require further low-pass or median filtering as well, since the noise is amplified in the derivatives. The system of equations has six unknowns, and as many equations as the number of image pixels used. Least squares fitting is used to find the values of each D and N. The bending stiffnesses, D_x and D_y, are of particular interest.

Field test

The measurement hardware was installed on a production machine. During the trial, the paper machine produced unbleached containerboard at a basis weight varied between 125 and 240 g/m². Data was collected during approximately 17 consecutive days. The hardware currently lacks online data processing algorithms; hence, the images were stored on a hard drive and processed later as they would be in an online setting. Due to the limitations of data storage, the frequency of acquiring images was lower than the maximum possible, at one image per 4 s. For this reason, only one result per reel of product was recorded so that the stochastic variations could be removed. As the camera capability is at least 10 images per second, by mean filtering the same number of images as in this test, one could expect at least 40 results per reel in an online application.

Reference and sample images were captured from all parts of the reel and tagged accordingly. The measurement vacuum that matched the sample images was also recorded. The vacuum was set to two constant values of control: a lower value for a lower weight of product (< 170 g/m²) and a higher value for a heavier product. (In actuality, the pressure experienced by the paper depends on its porosity.) This was done to ensure adequate bending

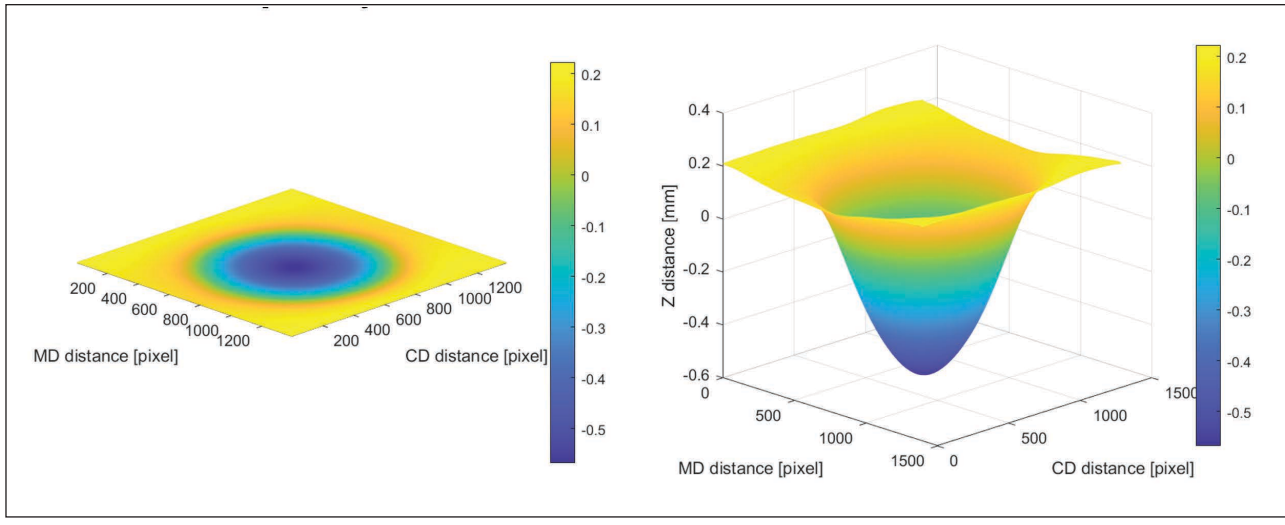

6. An integrated surface (scaled z-axis on right). Surface area is 34.8 mm x 34.8 mm. (MD = machine direction; CD = cross-machine direction.)

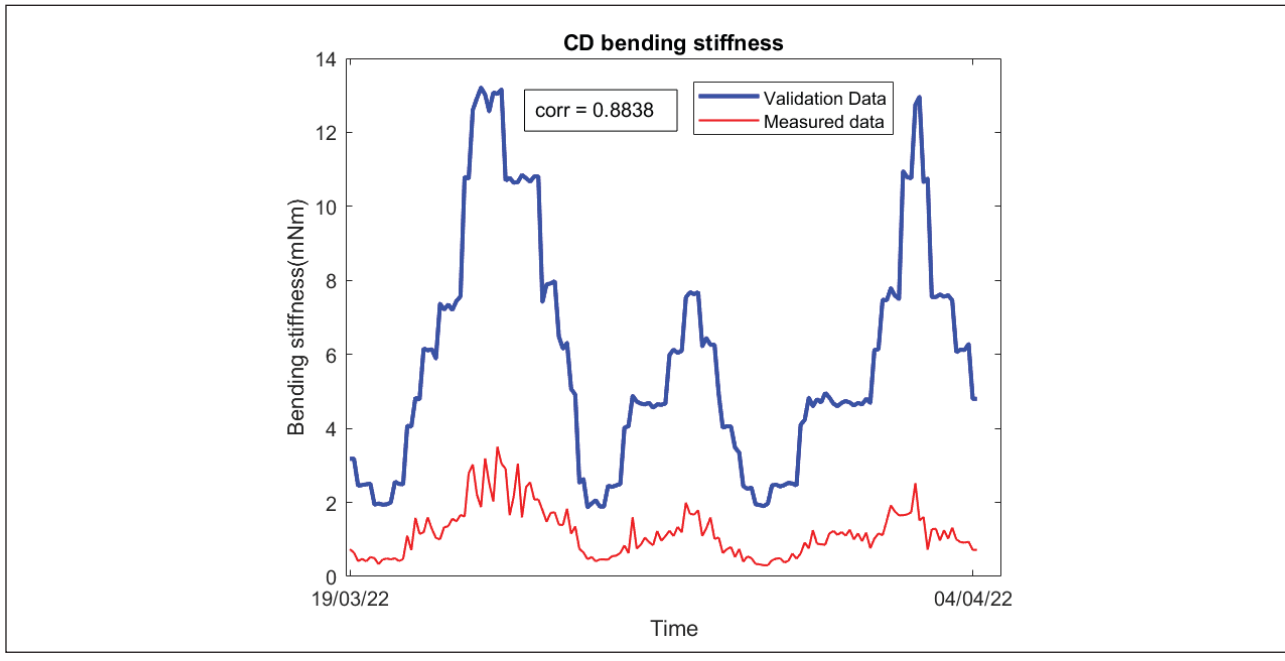

7. Online measured bending stiffness (mNm) in CD vs. laboratory results of bending stiffness. The fluctuation in time is due to manufacturing of different product grades (corr = correlation coefficient).

and to avoid the web detaching from the measurement vacuum hole with a stiff product, as well as to avoid breaking a lightweight product. Later, offline, all the reference images and sample images saved per reel were mean filtered to form their respective candidates, and one value per parameter (D and N) in Eq. 1 was solved.

State-of-the-art PaperLab's measurement techniques were conducted during the tests for results comparison. Laboratory results were obtained approximately once every three reels and include, among other things, the measured bending stiffness values of a product sample.

RESULTS AND DISCUSSION

The online measured bending stiffnesses in CD and MD directions are plotted against the corresponding laboratory-measured data in **Fig. 7** and **Fig. 8**, respectively. The online measured data has lower values than the laboratory data, and there is also significant noise in the measured data that has higher intensity in higher values of the properties. There exists correlation in the measured data and the laboratory results. The correlation coefficients are given in the figures. This correlation is also depicted in **Fig. 9** and **Fig. 10**, where the measured data has been given a constant gain and offset using least squares fit.

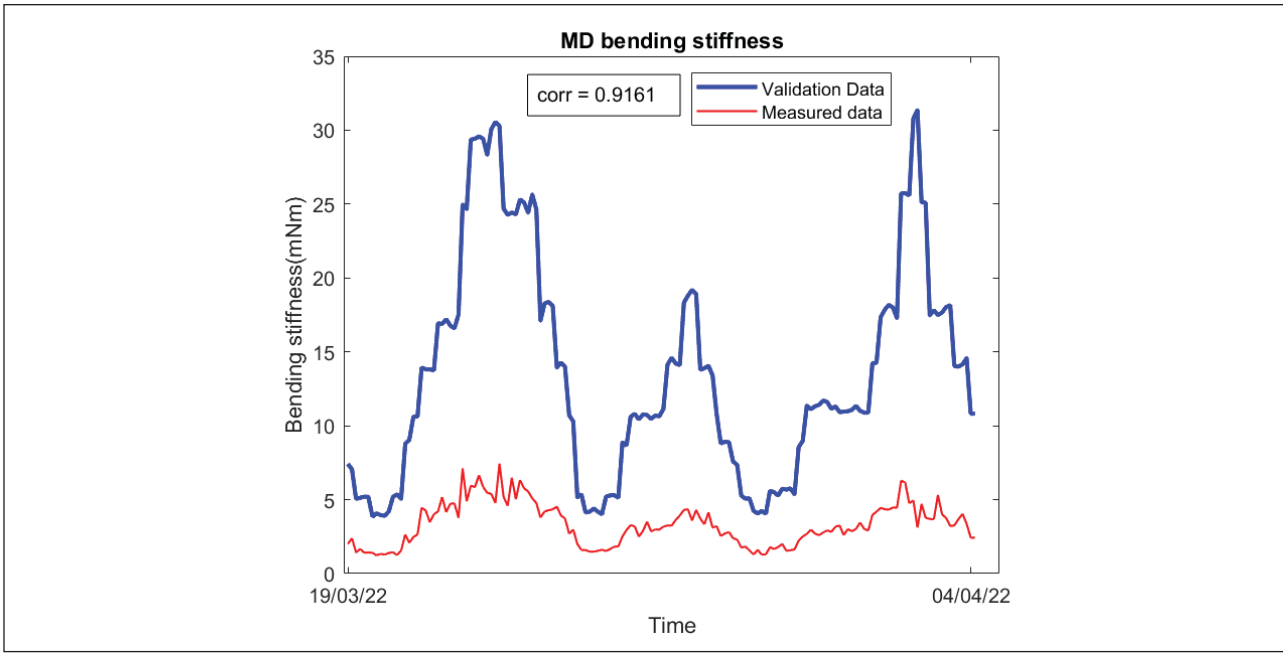

8. Online measured bending stiffness (mNm) in MD vs. laboratory results of bending stiffness. The fluctuation in time is due to manufacturing of different product grades (corr = correlation coefficient).

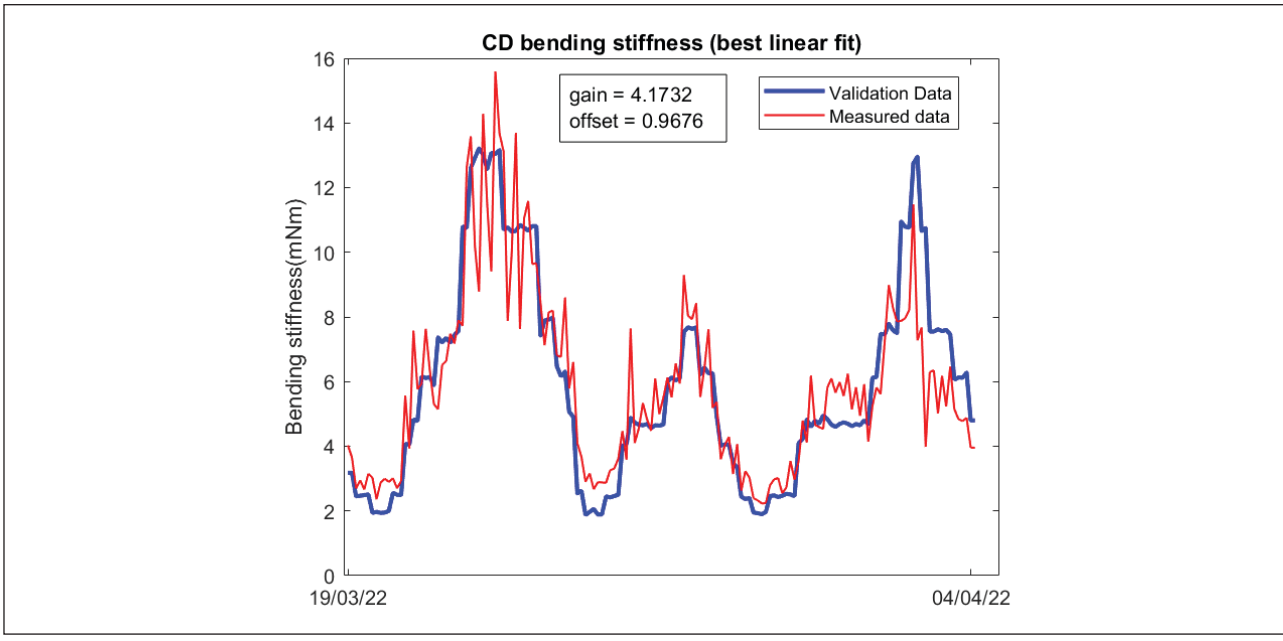

9. Online measured CD-specific bending stiffness (mNm) with gain and offset vs. laboratory results of bending stiffness. The fluctuation in time is due to manufacturing of different product grades.

These values are also given in the corresponding figures.

The MD tension is measured during manufacturing from the differences in reeling rates of the rollers (e.g., [13]). This property is compared to the MD tension solved from Eq. 1, and the results are plotted in **Fig. 11**. The former property is constant, at around 800 N/m, whereas the latter is fluctuating. These values should be compared with caution; the tension calculated from reeling rates is assumed to represent some average across the entire web between the rollers, whereas the measured value represents the tension within a small area of the sensor. It is unlikely that the tension due to reeling is spread evenly across the web. Also, contact with the measurement apparatus can cause significant change in local web tension.

Hypothesized error sources

Equation 1 provides an overview of the advantages and challenges of the approach presented in this study. It is

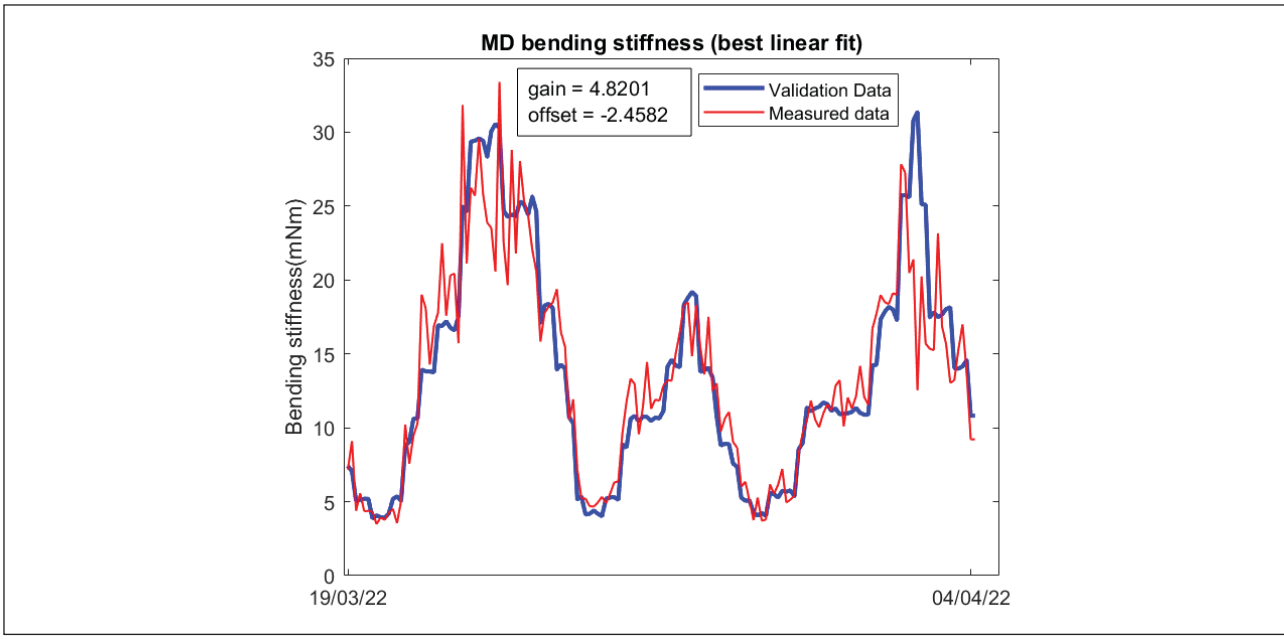

10. Online measured MD-specific bending stiffness (mNm) with gain and offset vs. laboratory results of bending stiffness. The fluctuation in time is due to manufacturing of different product grades.

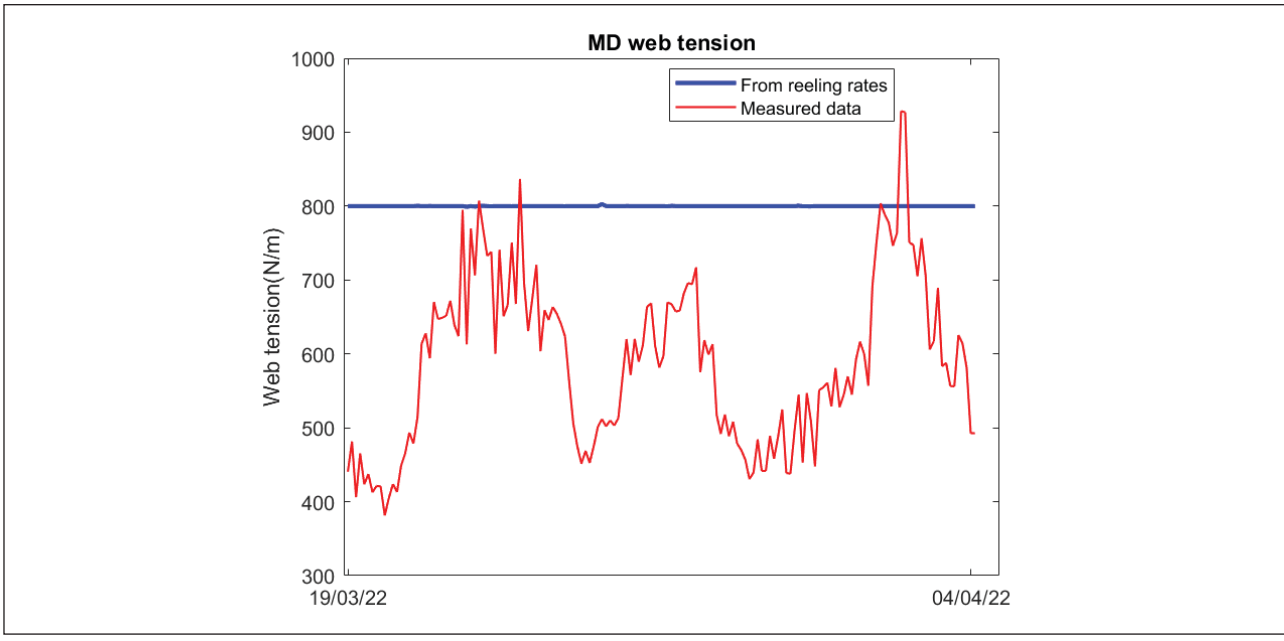

11. Online measured MD web tension (N/m) vs. tension calculated from reeling rates.

clear that several unknown parameters simultaneously affect the running paper web and vary in different CD positions and with respect to time. The reverse engineering approach presented in this paper, which directly measures and predicts the derivatives of the deflected surface, overcomes the challenges associated with determining boundary conditions that could be applied to an analytical solution. However, the derivatives are highly sensitive to small-scale variations due to imaging and paper surface topography. This effect accumulates in the higher order derivatives. Low-pass and median filtering is used to reduce noise, but filtering can have a detrimental effect on local shapes and thus derivatives.

Equation 1 contains seven unknown parameters related to the in-plane mechanical properties of the paper structure and web tension. There are also parameters and conditions that are not included in this equation and that have not been studied so far, e.g., terms related to the anticipated oscillations of the moving web (where the density of paper becomes a necessary variable). The large number of un-

known parameters implies the sensitivity of numerical analysis. It also suggests that a few measurement values, such as the maximum deflection or stresses at a few points, cannot provide a unique solution to the equation. This also explains the challenges associated with previous attempts. The single deflected surface measured in this study provides a vast number of equations that can be solved as an overdetermined system, providing the opportunity to solve multiple parameters, and also to homogenize local flaws either in the measurement technique or paper.

The governing equation is derived using several assumptions and approximations, some of which may not hold in practice: The deflections are presumed small; the maximum deflection should be less than one fifth of the thickness of the plate [14]. This is not the case in the conducted field tests. The direction coupling of the material's behavior is also simplified.

Another class of error source arises from the measurement conditions and performance of the measuring sensors. The paper not closing tightly to the edges of vacuum hole may cause noise to pressure level and deflected surface (shape). There is also known to exist some out-of- synchronization movement between the frame that houses the camera and the one that houses the porosity meter on the other side of the web. When mean-filtering these shifted images, the pixel grayscale intensities that form the calculated surface do not remain focused. This causes the surface shape to "blur." The pit-like shape caused by the vacuum then appears wider and less curved. All z-directional movement between sample surface and lights also affects the photometric stereo result of deflected shape. Also, the surface of the reference may not always be planar perpendicular to the z-axis. The unknown temperature and moisture content differences of the paperboard in laboratory and online measurement conditions, as well as CD streakiness and variations in moisture, tension, or other profile properties, are obvious sources for errors.

There is a clear trend that errors and noise increase in the case of heavier board grades. Several error sources mentioned earlier become more severe as basis weight and thickness increase. The structural topography variations increase compared to deflection applied and there is more surface roughness, which weakens the sealing of the web against the edge of the hole. When the ratio of thickness-to-vacuum hole dimensions increases, the validity of the governing equation reduces.

The scale difference in bending stiffness between laboratory and online results may be attributed to moisture differences, geometrical instability of the prototype, and filtering issues. Also, the validation method uses uniaxial loading and is not like the double-curved flexure of a plate as in the proposed method. The online measurements are also taken across the CD of the web, whereas laboratory measurements only use the middle portion. The paper's properties are known to vary, especially on the web edges.

Future improvements for industrial application

Several future improvements and test cases were discovered based on the hypothesized problems. More complex material models that consider larger deformations may be tested with the collected data. Alternatively, smaller vacuum pressure could be used, so that the deformations remain small enough to satisfy linear plate theory. In this case, however, the deformations due to unknown factors (i.e., web detaching from the measurement head, surface roughness, etc.) are more pronounced in comparison to those caused by the vacuum. An algorithm could be utilized to remove images from the mean filtering when these unknown factors are detected.

The distance between the web and measurement head can be adjusted to reduce the possibility of the web detaching. This comes with a risk of breakage, however. The frames housing the camera and the vacuum can also be focused with a laser pointer housed in the vacuum frame. The light from the laser hitting the paper is detected by the camera, and images are spatially synchronized, removing the effects of the relative frame movement.

The measurement frequency is significantly improved once the calculations are coded into the hardware. This will cause less noise due to surface roughness and other variations since more images are available for mean filtering. This will also allow separation of data measured from different CD positions, where the bending stiffness can have different values, especially on the edges.

Most state-of-the-art bending stiffness measurements are conducted by means of uniaxial bending. A measurement vacuum hole that is significantly longer in one dimension could reduce the axial bending coupling effects occurring in the proposed method. In this way, the two measurements are more comparable.

The industry accepts gain and offset fitting for measured data. Since the linear correlation between measured and validation data is strong, data-based learning methods may be used with the proposed measurement architecture, provided that the measurement does not require much calibration and that the noise can be reduced.

Further studies for optimizing the design, dimensions of instruments, and control parameters used in measurement are going to be conducted using data generated by the finite element method (FEM). Preliminary tests using FEM-modeled data of the case has shown that, in simple cases (anisotropic material, no web tension), the analysis is qualified, if the measurement data is selected far from the ignored reaction forces of boundary conditions.

CONCLUSION

The presented method, based on the analysis of data from deflected surface shape, offers a promising way to measure the bending stiffness in two directions. In conjunction, the level web tension from the moving web is solved.

Inevitably, several parameters affect the bending of the two-dimensional orthotropic plate in the online environment. The governing differential equation, derived using an approach of elastic flexure of an orthotropic plate, demonstrates the complexity of the situation. The analytical solution of the equation for the deflection profile is impossible to determine when the forces at real boundary conditions are unknown, as is the case in the study. However, the reverse engineering approach of this study, where the derivatives of the governing equation are calculated directly from the measured shape of deflected surface, allows the establishment of an overdetermined set of equations. These equations allow solving the bending stiffnesses and web tension values. The fourth order derivatives required to form these equations are sensitive to any kind of small-scale error or noise in the surface topography. This is one of the most significant challenges of the method, together with the challenge of ensuring sufficient accuracy of the material model.

The prototype of the measuring instrument was straightforward to implement, as it could be built by combining two existing online sensors, one developed to measure porosity and one to determine surface roughness. Despite the complexity of the phenomenon of paper deformation, solving the bending stiffnesses using the presented method only needs information about the pressure difference and the shape of the surface deflection.

There does not yet exist a specific goal for the accuracy of this novel method. Different state-of-the-art measurements for bending stiffness give different values for the same material. The goals of the method will likely depend on the method of validation and the desired parameter as per use case. Interest to correlate the measurement data with SCT also exists.

The first online trials with a paper machine were shown to give promising results. Good correlation between laboratory and online measurements were achieved for bending stiffnesses in MD and CD directions, although the observed noise in the data, especially with the heavier grades, was at a high level. Many issues remain to be studied and improved before practical application. The development of modeling, implementation algorithms, and hardware is ongoing. Finite element analysis will also be used to optimize the sensor's dimensioning and control parameters. The goal of the research is to develop a measurement technology for bending stiffness that is capable of providing estimates for feedback control in both MD and CD. **TJ**

ABOUT THIS PAPER

Cite this article as:
Salo, M., Erkkilä, A., Vilkko, M., et al., *TAPPI J.* 22(5): 344(2023). https://doi.org/10.32964/TJ22.5.344

DOI: https://doi.org/10.32964/TJ22.5.344

ISSN: 0734-1415

Publisher: TAPPI Press

ABOUT THE AUTHORS

This topic was suggested by Valmet Automation as the subject of my (Salo's) doctoral thesis. The topic was studied prior to starting my thesis by Valmet Automation and Anna-Leena Erkkilä. Other previous research has tried to solve the problem, with no widespread use yet in practice. Here, we attempt to solve similar problems with a different approach.

The most difficult aspect of this study was that paper strength properties are difficult to solve and depend on many variables. Our method addresses some, but others remain to be studied. However, it was interesting to see that the data correlation was quite high.

Many mills are currently interested in this method. They desire faster monitoring of the properties, as well as feedback control of them. Research and development with our industry partner and their clients are ongoing. The next step is model, hardware, and algorithm development, as well as more tests with plant data and simulated data.

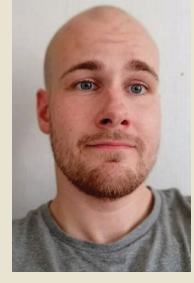

Salo

Erkkilä

Vilkko

Kanerva

Salo is a doctoral researcher, Vilkko is professor, and Kanerva is associate professor at Tampere University in Tampere, Finland. Erkkilä is R&D engineer at Metsä Board in Jyväskylä, Finland. Email Salo at mikko.salo@tuni.fi.

LITERATURE CITED

1. Kirwan, M.J., *Handbook of Paper and Paperboard Packaging Technology*, John Wiley & Sons, Chichester, UK, 2013. https://doi.org/10.1002/9781118470930.
2. Niskanen, K., *Papermaking Science and Technology. Book 16, Paper Physics*, Finnish Paper Engineers' Association/Paperi ja Puu Oy, Jyväskylä, Finland, 2008.
3. Chase, L., Goss, J., and Anderson, L., *Tappi J.* 72(12): 89(1989).
4. Chase, L., Cresson, T., Goss, J., et al., *Tappi J.* 76(10): 37(1993).
5. Reed, W. and Brown, T., *Pulp Pap.* 73(3): 61(1999).
6. Senko, E. and Thorpe, J., *Tappi J.* 68(2): 95(1985).
7. Vahey, D.W., *Tappi J.* 70(3): 79(1987).
8. Kažys, R. and Stolpe, P., *NDT&E Int.* 34(4): 259(2001). https://doi.org/10.1016/S0963-8695(00)00066-9.
9. Allan, R.J., *Appita J.* 68(3): 211(2015). https://doi.org/10.1080/00131911.2015.1058752.
10. Baum, G.A. and Habeger, C.C., *Tappi* 63(7): 63(1980)
11. Jong, J.H., Brodeur, P.H., and Gerhardstein, J.P., *1999 Int. Pap. Phys. Conf.*, TAPPI Press, Atlanta, p. 19.
12. Anttila, J. and Pettersson, T., *Meas. Sci. Technol.* 8(8): 921(1997). https://doi.org/10.1088/0957-0233/8/8/014.
13. Valenzuela, M.A., Bentley, J.M., and Lorenz, R.D., *IEEE Trans. Ind. Appl.* 39(2): 294(2003). https://doi.org/10.1109/TIA.2003.809449.
14. Hakim, G. and Abramovich, H., *Materials* 15(4): 1577(2022). https://doi.org/10.3390/ma15041577
15. Gevers, T., Gijsenij, A., Van de Weijer, J., et al., *Color in Computer Vision: Fundamentals and Applications*. John Wiley & Sons, Hoboken, NJ, USA, 2012. https://doi.org/10.1002/9781118350089.
16. Shi, B., Matsushita, Y., Wei, Y., et.al., *Comput. Soc. Conf. Comput. Vision Pattern Recognit.*, IEEE, New York, 2010, p. 1118.
17. Chakrabarti, A. and Sunkavalli, K., *Fourth Int. Conf. 3D Visio*n, IEEE, New York, 2016, p. 258.
18. Frankot, R.T. and Chellappa, R., *IEEE Trans. Pattern Anal. Mach. Intell.* 10(4): 439(1988). https://doi.org/10.1109/34.3909.
19. Wang, C.M., *Shear Deformable Beams and Plates Relationships with Classical Solutions*, Elsevier, Amsterdam, 2000.
20. Timoshenko, S., *Theory of Plates and Shells*, McGraw-Hill, New York, 1959.

APPENDIX A

Single-image photometric stereo with a reference calibration

Specific surface with double curvature can be determined by photometric stereo using three or more light sources that are positioned in different azimuth directions with respect to the object. The method is based on Lambert's cosine law. It is assumed that the intensity of the light reflected by the surface, I, is proportional to the dot product of the surface normal, n, and the direction of a point light source, L. The intensity of the reflected light is assumed the same in all outward directions. The equation for reflected intensity is [15]:

$$I = [L \cdot n]\, k(\lambda)\, I_0 \tag{1}$$

where $k(\lambda)$ is the surface albedo (which is a material property and a function of the light wavelength) and I_0 is the light intensity received by the surface.

A digital camera observes an area of X times Y pixels. The signal $c(i)$ observed by the camera for each pixel $i \in X \times Y$ is proportional to to the light intensity reflected by the surface area of the pixel:

$$c(i) = b(i)\, I(i) = b(i)\, [L(i) \cdot n(i)]\, k(\lambda, i)\, I_0(i) \tag{2}$$

where $b(i)$ depends on parameters such as camera sensitivity and optical system transmittance. A similar model has been used for the example in [16].

For a reference image, r, planar in the xy-plane, we have:

$$\left[L^{(r)}(i) \cdot n^{(r)}(i)\right] = L_z^{(r)}(i) \tag{3}$$

since $n^{(r)} = [0,0,1]^{\mathrm{T}}$. Furthermore, if the deviations in the z-component of the surface are small in comparison to the distance of the light sources, then $L(i)$ and $I_0(i)$ are practically the same for a planar reference surface and a slightly deformed surface.

For any image, c, of a slightly deflected (from the xy-plane) surface, S, and reference image, $c^{(r)}$, of a planar surface, we have:

$$\begin{aligned} F(i) \;&:= \frac{c(i)}{c^{(r)}(i)} \\ &= \frac{b(i)\, [(L(i) \cdot n(i)]\, k(\lambda, i)\, I_0(i)}{b(i)[(L(i) \cdot n^{(r)}(i)]\, k^{(r)}(\lambda, i)\, I_0(i)} \\ &= \frac{[(L(i) \cdot n(i)]}{L_z(i)}, \end{aligned} \tag{4}$$

where it has been presumed that the reference and sample are taken with the same material and the albedo does not

change. Using red, green, and blue (RGB) lights, we obtain a system of equations:

$$\begin{bmatrix} L_z^R F^R \\ L_z^G F^G \\ L_z^B F^B \end{bmatrix} = \begin{bmatrix} L_x^R & L_y^R & L_z^R \\ L_x^G & L_y^G & L_z^G \\ L_x^B & L_y^B & L_z^B \end{bmatrix} \begin{bmatrix} n_x \\ n_y \\ n_z \end{bmatrix} \tag{5}$$

Every variable in Eq. 5 is a function of *i*, which is left out to shorten the notation. The left side of Eq. 5 is abbreviated *F(i)* and is obtained from reference and sample data measured by the camera and known system geometry, as suggested by Eq. 4. For each pixel *i*, the light direction matrix, Eq. 6, can be calculated from known system geometry:

$$\mathcal{L}(i) := \begin{bmatrix} L_x^R(i) & L_y^R(i) & L_z^R(i) \\ L_x^G(i) & L_y^G(i) & L_z^G(i) \\ L_x^B(i) & L_y^B(i) & L_z^B(i) \end{bmatrix} \tag{6}$$

If the three light directions are chosen in a way that the system of equations (Eq. 5) has full rank, we have:

$$n(i) = \mathcal{L}(i)^{-1} \mathcal{F}(i) \tag{7}$$

Either multiple cameras or multiple images under different light directions are required in photometric stereo. Different, distinguishable wavelength lights may also be used. This requires solving for three albedos, however. A similar approach for obtaining certain surface form using RGB photometric stereo has been used in some works [17]. In our case, the calibrating reference image is taken from the same material and system geometry, hence the albedo and light intensities received by the pixels are factored out and the problem is much less complicated. The benefit of using three lights that can be distinguished by the camera is that one image provides more data.

Any 2-D surface can be represented as a parametrization $r(x,y) = (x, y, w(x,y))$, where $w(x,y)$ is a function that returns the z-component of the surface for each point (x,y). For the normal n of a parametrized surface at each point (x,y), it holds that:

$$n = \frac{\partial r}{\partial x} \times \frac{\partial r}{\partial y} = \begin{bmatrix} -\dfrac{\partial w}{\partial x} \\ -\dfrac{\partial w}{\partial y} \\ 1 \end{bmatrix} \tag{8}$$

Hence, for *S*, we have:

$$\begin{aligned} \frac{\partial w}{\partial x}(i) &= -\frac{n_x(i)}{n_z(i)} \\ \frac{\partial w}{\partial y}(i) &= -\frac{n_y(i)}{n_z(i)}, \end{aligned} \tag{9}$$

where *w(i)* is the height profile of the surface for each pixel *i*. Using the partial derivatives, the shape of the surface can be integrated using various methods [18].

APPENDIX B

Small deflections of thin plates

For deformations in the linear-elastic region of orthotropic material, the stress components, σ, and strain components, ϵ, are related by:

$$\begin{aligned} \epsilon_{xx} &= \sigma_{xx}/E_x - \nu_{yx}\,\sigma_{yy}/E_y - \nu_{zx}\,\sigma_{zz}/E_z, \\ \epsilon_{yy} &= \sigma_{yy}/E_y - \nu_{xy}\,\sigma_{xx}/E_x - \nu_{zy}\,\sigma_{zz}/E_z, \\ \epsilon_{zz} &= \sigma_{zz}/E_z - \nu_{xz}\,\sigma_{xx}/E_x - \nu_{yz}\,\sigma_{yy}/E_y, \end{aligned} \tag{10}$$

where each *E* refers to the stiffness, namely Young's modulus, of each direction. Similarly, each ν refers to the Poisson's ratio between two directions. It is presumed that shear deformation is uncoupled. For the shear stresses, τ, and shear strains, γ, we have:

$$\begin{aligned} 2\gamma_{yz} &= \tau_{yz}/G_{yz}, \\ 2\gamma_{zx} &= \tau_{zx}/G_{zx}, \\ 2\gamma_{xy} &= \tau_{yz}/G_{xy}. \end{aligned} \tag{11}$$

Here, no coupling between in-plane and out-of-plane deformation will be considered, i.e.:

$$\begin{aligned} \sigma_{xx} &= E'_x\,\epsilon_{xx} + E''\,\epsilon_{yy} \\ \sigma_{yy} &= E'_y\,\epsilon_{yy} + E''\,\epsilon_{xx} \\ \tau_{xy} &= 2G_{xy}\,\gamma_{xy} \end{aligned} \tag{12}$$

with the notation:

$$\begin{aligned} E'_x &= E_x/(1 - \nu_{xy}\,\nu_{yx}), \\ E'_y &= E_y/(1 - \nu_{xy}\,\nu_{yx}), \\ E'' &= \nu_{yx}\,E_x/(1 - \nu_{xy}\,\nu_{yx}) = \nu_{xy}\,E_y/(1 - \nu_{xy}\,\nu_{yx}). \end{aligned} \tag{13}$$

The plate is affected by transverse (out-of-plane) force per unit area, *q*, normal to the surface of the plate in the

z-direction, as well as in-plane force per unit length (N) affecting in plate's x and y directions. The situation is depicted in Fig. 1. The transverse forces cause deflection, w, in the z-direction, and we assume that these deflections are small in comparison to the thickness of the plate.

The flexural deformation of the plate is assumed to follow the Kirchoff's plate theory, where shear deformations are ignored with respect to the planes parallel to the neutral plane of the plate. (In this case, the neutral plane is the middle plane of the plate in the xy-plane.) Also, straight lines normal to the neutral plane remain straight and normal upon flexure. If the angle of the deflection with the xy-plane is small, the relationship between strains and the distribution of w can then be approximated by [19]:

$$\epsilon_x = -\hat{z}\frac{\partial^2 w}{\partial x^2}, \quad \epsilon_y = -\hat{z}\frac{\partial^2 w}{\partial y^2}, \quad \epsilon_{xy} = -2\hat{z}\frac{\partial^2 w}{\partial x\,\partial y} \tag{14}$$

where $\hat{z}$ is the distance of a point from the neutral plane of the plate.

Here, material is assumed homogeneous in the thickness direction, but directional in the xy-plane. This means that the elastic properties in different directions may differ. It is assumed that the edges of the plate are free to move in the plane of the plate at the boundary of w. With these assumptions, the governing differential equation of deformation becomes [20]:

$$\begin{aligned} q \quad &= D_x\frac{\partial^4 w}{\partial x^4} + 2\left(D_1 + 2D_{xy}\right)\frac{\partial^4 w}{\partial x^2\,\partial y^2} + D_y\frac{\partial^4 w}{\partial y^4} \\ &-N_x\frac{\partial^2 w}{\partial x^2} - 2N_{xy}\frac{\partial^2 w}{\partial x\,\partial y} - N_y\frac{\partial^2 w}{\partial y^2}, \end{aligned} \tag{15}$$

where:

$$D_x = \frac{E'_x\,h^3}{12}, \quad D_y = \frac{E'_y\,h^3}{12}, \quad D_1 = \frac{E''\,h^3}{12}, \quad D_{xy} = \frac{G\,h^3}{12} \tag{16}$$